



ORIGINAL ARTICLE

Facile preparation of Fe₂O₃ nanoparticles mediated by *Centaurea alba* extract and assessment of the anti-atherosclerotic properties



Jian Xiu^a, Ying Zhang^{b,*}, Bilal Ahamad Paray^c, Aneela Gulnaz^d, Mehraj Ud Din War^e

^a Department of Cardiology, First People's Hospital of Zhaoqing, Zhaoqing, Guangdong Province 526000, China

^b Department of Cardiology, Suqian Hospital of Integrated Traditional Chinese and Western Medicine, Suqian, Jiangsu Province 223800, China

^c Department of Zoology, College of Science, King Saud University, P.O. Box 2455, Riyadh 11451, Saudi Arabia

^d College of Pharmacy, Woosuk University, Wanju-gun 55338, Republic of Korea

^e PG And Research Department of Zoology, The New College (Autonomous), Chennai 600014, India

Received 3 August 2021; accepted 7 October 2021

Available online 16 October 2021

KEYWORDS

Atherosclerosis;
Iron oxide nanoparticles;
Centaurea alba;
Hypercholesterolemia;
Lipid profile

Abstract This research work attempts to synthesize iron nanoparticles with *Centaurea alba* extract. The reported synthesis method serves to be more effective over conventional physical and chemical methods, which is found to be cost effective, recyclable, biocompatible and prevents oxidation of iron oxide nanoparticle as well. As the extract of *Centaurea alba* possess high content of flavonoids, tannins and phenolic acids, it thereby prevents the oxidation and accumulation iron oxide NPs. The morphological features of the obtained nanoparticle were determined by TEM and SEM imaging techniques. Furthermore, various spectroscopic techniques including UV-Vis, FT-IR has been evaluated. As a part of cellular and molecular studies, the prepared FeNPs was subjected to MTT assay for 48h on normal (HUVEC) cells to evaluate its cytotoxicity. The IC₅₀ of FeNPs and BHT against DPPH free radicals were 287 and 191 µg/mL respectively. Male Wistar rats were selected as the model organism for the in vivo studies and has been categorized into 6 groups, where normal diet was provided to the control group, cholesterol diet was provided to sham group (HCD: 1.50% cholesterol and 24.00% fat) and HCD was provided to other groups. FeNPs were infused at low (100µg Kg⁻¹), moderate (200 µg/Kg) and maximum (400 µg/Kg) doses via gavages. Additionally, atorvastatin (10 mg Kg⁻¹) was provided to the last group through gavages with HCD. Six months has been fixed as a study period for all the groups. Various parameters

* Corresponding author.

E-mail address: zhangyingsci@sina.com (Y. Zhang).

Peer review under responsibility of King Saud University.



including total cholesterol (TC), low-density lipoprotein cholesterol (LDL-C), triglyceride (TG) and high-density lipoprotein cholesterol (HDL-C) was assessed in the blood samples of the test organism at the end of the period. Furthermore, sections of coronary artery and aortic arteries were subjected to histopathological examinations, which showed increase in vessel wall thickness in HCD group, however FeNPstreated groups showed no significant pathological changes. Decrease in TG, TC and LDL-C was observed upon treatment of HCD animals with FeNPs.

© 2021 Published by Elsevier B.V. on behalf of King Saud University. This is an open access article under the CC BY-NC-ND license (<http://creativecommons.org/licenses/by-nc-nd/4.0/>).

1. Introduction

Centaurea, being one of the largest plant species with over 700 diverse species (Nemorosa, 2017), usually grows up to two meters and generally found in different parts of Asian countries (Mosaddegh et al., 2018). It is mainly exploited in ancient traditional medicines (Fatima, et al., 2019; Bensouici, 2012). Studies have reported the presence of diverse type of organic compounds in the *Centaurea aura* leaf extract which includes lactones (Öksüz and Ayyildiz, 1986), flavone (Oksuz, 1982) flavonoid (Esmaeili, 2013), lignans and alkaloids (Harper, 2002). Moreover, this species has reported to have anti-microbial, anti-cancer and antioxidant properties (Khan, 2011; Ghashghaii et al., 2017). Literatures shows strong evidence about the enhancement of therapeutic properties of metallic nanomaterials when they are green synthesized by antioxidants rich ethnomedicinal plants (Abdoli et al., 2020; Sujayev et al., 2020; Hummers and Offeman, 1958; Kooti et al., 2017).

Metallic nanoparticles are well-known for its ability of binding non-destructively to single-stranded DNA, which is considered as an important aspect in medical diagnostics. Moreover, nanomaterials can make its way through the vessels and successfully place its target, which is widely exploited in imaging, biomedicine and other therapeutics (Abdoli et al., 2020; Sujayev et al., 2020; Hummers and Offeman, 1958; Kooti et al., 2017). Nanomaterials are widely used in various biomedical applications as drug carriers, carriers for gene therapy, hyperthermia and materials for MRI (Sujayev et al., 2020; Hummers and Offeman, 1958). For the effective use of nanoparticle for delivery of drug molecule or DNA fragments for gene therapy, surface modification of nanoparticle is required for specific interaction with the targeted biomolecule. These surface modified nanomaterials eventually used for in vitro and in vivo chemical processes. Among a wide array of nanomaterials, metal nanoparticles are widely preferred owing to their antifungal, UV absorbing properties and photocatalytic activity (Abdoli et al., 2020; Sujayev et al., 2020; Hummers and Offeman, 1958). Their anti-bacterial properties extend their application to food industry and active food packaging. Potential utilization of metallic nanoparticles are exploited for hyperthermia, tumor treatment, biomarkers, biodegradation and for the removal of organic, inorganic and radioactive contaminants (Sujayev et al., 2020; Hummers and Offeman, 1958; Kooti et al., 2017; Shanzha, 2018; Arunachalam, 2003; Pashaie et al., 2017).

Being a strong antioxidant, metallic nanoparticles are less toxic than the metals and has greater potential of free radical scavenging, which makes them a natural antioxidant. Literatures have reported at cytoplasmic and mitochondrial level, nanoparticles detoxify hydroperoxides and lipo-peroxidases.

Iron, silver, titanium and copper based metallic nanoparticles possess high antimicrobial properties which could be used in biomedical and industrial sectors (Ghashghaii et al., 2017; Abdoli et al., 2020; Sujayev et al., 2020). Nanoparticles are being coated to ensure target specificity, among which peptides are considered as the best choice (Ghashghaii et al., 2017; Abdoli et al., 2020; Sujayev et al., 2020; Hummers and Offeman, 1958; Kooti et al., 2017).

In the current research, we investigated the facile preparation of Fe nanoparticles mediated by *Centaurea alba* extract and its anti-atherosclerotic properties in the *in vivo* condition.

2. Material and methods

2.1. Materials

The *Centaurea alba* plant, which is applied in this study as a factor for reducing metal ions and stabilizing nanoparticles, has been prepared. FeCl₃·6H₂O, ethanol and methanol were purchased from Merck.

2.2. Preparation and extraction of aqueous extract

First, it was necessary for the experiments to provide a pure solution of the extracts of the leaves of *Centaurea alba* plant. To do this, 1.5 g of leaf powder was added to 60 mL of deionized water. Then, the resulting solution is placed on a hot plate at 60° C for 2.5 h to dissolve plant agents and metabolites well in the solvent. The resulting solution was poured into the Falcon tubes, and centrifuged at 5000 rpm for 10 min to separate the plant residue from the extract. Then, the resulting extract was moved into test tubes, and placed in the refrigerator to keep it fresh and healthy.

2.3. Green synthesis and chemical characterization of iron nanoparticles

Various factors were involved in the synthesis of Iron nanoparticles (FeNPs). These factors include temperature, time, and concentration of iron and volume ratio of iron solution to extract solution. Different experiments were designed and tested to achieve the optimal conditions for each of these factors. During the complete duration of the experiment, the concentration of the extract was kept constant. In a typical procedure, 2 mL of the prepared extract solution was diluted in 30 mL of deionized water. Then, 20 mL of FeCl₃·6H₂O solution (0.001 M) was added to the extract solution with a volume ratio of 1 to 1.5 mL and the mixture was placed on a hot plate at 60 °C while being mixed. After 30 min of the reaction time,

the color of the reaction solution changes completely and the synthesized nanoparticles collect as sediment at the bottom of the reaction vessel.

Different spectroscopic and imaging techniques were used to evaluate and identify the FeNPs. At the first step, UV–vis spectrum (Cary UV–Vis 4000, Agilent) was used to identify iron nanoparticles. Typically, iron nanoparticles have two absorption spectra in the range of 200–300 nm. The FTIR spectrum (PERKIN-ELMER, RXI) was used to identify nanoparticles and plant metabolites in plant extracts. Electron microscope techniques such as SEM (LEO 1430VP, UK) and TEM (H9500, HITACHI) were also used to examine the shape and size of nanoparticles.

2.4. Antioxidant activities of FeNPs

Degree of decolorization of the 2 and 2-diphenyl-1-picrylhydrazyl purple solution corresponds to the ability of the hydrogen atoms or electrons to give off different compounds and nanoparticles in the test solution, where DPPH was used a stable radical compound. Thus, 100 µl of various dilutions of nanoparticles in methanol was added to 10 mL of 0.005% DPPH solution in methanol. The samples were analyzed against blank at 518 nm after incubating it for an hour at room temperature. The formulae mentioned below depict the DPPH inhibition percentage (Abdoli et al., 2020):

$$\text{Inhibition(\%)} = \frac{\text{SampleA.}}{\text{ControlA.}} \times 100$$

In this formula, “Control A” shows the negative control of light absorption that lacks nanoparticles, and “Sample A” expresses the amount of light absorption of different concentrations of nanoparticles (Arunachalam, 2003).

2.5. Cytotoxicity potentials of FeNPs

MTT assay serves as a quantitative technique for the determination of live cell population. It is well known that live cells could do oxidative metabolism, in case of MTT assay, the oxidative process leads to the breaking down of MTT dye and results in producing a dye ranging from yellow to blue (Pashaie et al., 2017).

In this research, we used the HUVEC cell line (Human normal cell line) to evaluate the cytotoxicity effects of FeNPs using an MTT method.

To prevent the fungal growth, the cells were maintained in a DMEM medium with 1% penicillin/streptomycin antibiotic and 10% bovine embryos. Temperature of 37 °C and 5% CO₂ with 95% moisture are considered ideal for cell growth, which was provided by the NÜVE incubator (EC160 model). When the cell reaches 70% of cell growth, they were separated from the flask by using trypsin-ethyl diamine tetraacetic acid and has been centrifuged for 1–6 min at 1700 rpm. Cell precipitate was prepared in suspension in 1 ml of culture medium. The cell suspension was scrutinized to determine its viability by mixing them with equal proportion of tryptan blue and the cells were counted with a neobar slide under light microscope. After confirming the infectivity of the cells, cells with 90% viability was proceeded for further process (Pashaie et al., 2017).

Tetrazolium salt calorimetric method (MTT) as exploited to investigate the effect of nanoparticles on proliferation. For

this test, 10⁴ cells were added to each 96-well plate well. The cells were incubated for 24 h and concentration of 1–1000 µg/mL was treated on cancer and normal cells for 24, 48 and 72 h.

After these times, 20 µl of MTT solution and 200 µl of base culture medium were added to each well. The plate was then placed at 37°C in dark CO₂ incubated for about 4 hours in the dark. After the incubation, each well was filled with 100 microliters of DMSO, where the optical readings were taken at 492 nm and 630 nm using the ELISA. The cell viability can be evaluated by the below expression (Pashaie et al., 2017):

$$\text{Cellviability(\%)} = \frac{\text{SampleA.}}{\text{ControlA.}} \times 100$$

2.6. Anti-atherosclerotic potentials of FeNPs

2.6.1. Animals and hypercholesterolemia induction

Wister rats, specifically adult healthy males with an average weight around 200–250 g were selected for the study. Pellet diet was followed for all the test animals and water was provided ad libitum. Standard environmental condition including temperature (24 ± 2 °C), relative humidity (45 – 55%) and dark/light cycle 12/12hr were followed to acclimatize the rats for a period of 7 days. The guidelines of ethical committee was followed for performing experiments on animals. The 24 weeks old male rats were fed with a high cholesterol diet (HCD) for six months. Hypercholesterolemia was induced as described previously, with the addition of dried egg yolk (50.00%) to the whole feed and providing diet with 1.50% cholesterol and 24.00% fat. Also, 0.20% propylthiouracil (PTU) was added to the daily diet in order to decrease the amount of thyroid hormone produced by thyroid gland and block the conversion of thyroxine to T₃. Thyroid hormone directly promotes cholesterol metabolism by the liver and PTU induces high blood levels of cholesterol. Stationary laboratory diet was followed to feed the control groups (El-Moslamy, 2017).

Experimental design. Before the experimental procedures, rats were randomly divided into control and test groups (n = 6) as follows:

Group I (Control): The control group animals received normal saline (1 mL per rat) via gastric tubes for six months; Group II: Sham group animals were categorized as group II and has received hypercholesterolemic diet for 6 months. Group III: Hypercholesterolemic diet and 100 µg kg⁻¹ FeNPs were fed to the animals via gastric tubes for six months; Group IV: hypercholesterolemic diet and 200 µg kg⁻¹ FeNPs was fed to the rats via gastric tubes for six months; Group V: the animals in this group were received hypercholesterolemic diet and 400 µg kg⁻¹ FeNPs via gastric tubes for six months and Group VI: the animals were received hypercholesterolemic diet and Atorvastatin (STN) (10 mg kg⁻¹) via gastric tubes for six months (El-Moslamy, 2017).

2.6.2. Serum preparation, tissue samples collections, and lipid profile measurement

Blood samples were directly collected from the heart of the animals following anesthesia with diethyl ether. Sera was obtained from the samples by centrifuging at 3000 g for 10 mins, which was then stored at -20 °C for further analysis. Anesthetized animals were humanely euthanized using CO₂

gas in a special device and immediately the heart and aorta were removed and rinsed with chilled normal saline. For pathological examinations, the samples were fixed in 10% phosphate buffered saline (PBS) formalin (El-Moslamy, 2017).

Concentrations of total cholesterol (TC), total triglycerides (TG), high-density lipoprotein cholesterol (HDL-C) and low-density lipoprotein (LDL-C) in serum were determined by enzymatic colorimetric methods using commercial kits (El-Moslamy, 2017).

2.6.3. Histopathological analysis

For histological studies, the samples of heart and aorta were fixed in 10% paraformaldehyde. Ethanol was used to dehydrate the tissues and cleared in toluene. Molten paraffin wax was used to embed the tissues. For microscopic analysis, the tissues were cut at 5 μm thickness and has been stained with eosin (H and E) and hematoxylin. Heidenhain's Azan trichrome staining was performed to show connective tissue, especially muscle, collagen and nuclear chromatin in histological sections. Changes in aortic wall and coronary arteries were studied by this method (El-Moslamy, 2017).

2.7. Statistical analysis

To compare the results, in addition to the formula mentioned above, which was calculated as an average of 5 repetitions of experiments. The results were analyzed using SPSS software version 22 and the statistical differences between the treatments were examined by *t*-test and $P \leq 0.01$ was considered significant.

3. Results and discussion

3.1. Chemical characterization of FeNPs

3.1.1. Nanoparticle analysis using UV-Vis spectroscopy

The effect of reaction temperature, time of the reaction, iron concentration and amount of extract solution on the synthesis of FeNPs were investigated using UV-Vis spectroscopy. The results are presented in Fig. 1. In each experiment one of the factors was evaluated while the other factors were kept constant. According to the results, the optimum condition for preparation of FeNPs was 0.001 M FeCl_3 solution, 1.5 vol ratio of extract solution to Iron solution, 60 °C and 30 min reaction time.

3.1.2. Analysis of FeNPs using FT-IR spectroscopy

FT-IR technique is another qualitative method in characterization of nanoparticles. The presences of the bands in the specific wavenumber regions shows useful information about the metallic nanoparticles. For example, if the nanoparticles are formed as metal oxide, the peaks at 400 to 700 cm^{-1} belong to metal oxygen bond. The presences of the peaks at the other region are attributed to the different bonds for organic compounds present in the plant extract that bind to the NPs. The FT-IR spectra of AgNPs is shown in Fig. 2. The peaks at wavenumbers of 437, 530, and 5581 cm^{-1} belong to Ag-O bond. Literatures has stated the peaks for green synthetic AgNPs with a little difference in wavenumber (Karpagavinayagam and Vedhi, 2019; Yazdani, 2019; Ting

and Yien, and Jia En Chin, 2020; Fazlzadeh, 2017). Moreover, the peaks at 3490 and 2979 cm^{-1} (O-H and aliphatic C-H stretching), 1480 to 1751 cm^{-1} (C = C and C = O stretching), (1031 cm^{-1} -C-O stretching) belong to the various bonds of organic compounds in *A. maurorum* extract that exist as the plant secondary metabolites. These compounds can be comprised different class of compounds such as phenolic, flavonoid, triterpenes, which were reported previously (El-Moslamy, 2017; Karpagavinayagam and Vedhi, 2019; Yazdani, 2019; Ting and Yien, and Jia En Chin, 2020; Fazlzadeh, 2017; Katata-Seru, 2018).

3.1.3. Analysis of nanoparticles using FESEM and TEM images

To study the morphological features and the size of the obtained FeNPs, FESEM was exploited. Fig. 3 shows the FESEM image of FeNPs. It could be observed from the figure that the obtained NPs exhibits spherical morphology, where their size range from 10-52 nm.

Fig. 4 shows the TEM image of FeNPs. The nanoparticles are surrounded by a thick layer of plant organic molecules, which reduces the image resolution of the nanoparticles. These observations are very similar to the observations in other research (Alam, 2019; Devatha et al., 2018; Önal, 2017; Bibi, 2019; Veisi et al., 2019).

3.2. Cytotoxicity, antioxidant, and anti-atherosclerotic activities of FeNPs

Examining the rate of survival, mortality and proliferation under various conditions has become crucial for the determination of cytotoxic effects. Cytotoxicity tests are carried out to assess the effects of various compounds in the cell. Being a non-radioactive colorimetric system, MTT assay greatly contributed to biocompatibility studies of various materials. In MTT analysis according to ISO 10993-5 international standard, different equipments are tested for cytotoxicity, if they do not have toxic effects, they will obtain the necessary standards and licenses and enter the buying and selling market. For testing the cell viability, MTT assay has been considered to be ideal. The primary aim and role of the MTT assay is to assess the toxic effect of compounds, drugs or other supplements. It has also been mentioned as a method used for the determination of cell proliferation or counting in numerous literatures (Tahvilian et al., 2019; You et al., 2012; Mao, 2016; Beheshtkhoo et al., 2018). By affecting the intracellular organs, MTT analysis provides the difference between live and dead cells. In this assay, the cultured cells are treated with desired compounds to evaluate its toxicity. The cell viability was determined for each concentration of the substance. Even though the method is primarily used for water-soluble compounds, it has been recently used for components soluble in organic solvents as well. Hormones, cytokines, growth factors and mitogens greatly influence the behavior and rate of cell proliferation. Moreover, some drugs, usually those which are cytotoxic, results in necrosis or apoptosis of cells or even decrease the cell proliferation rate (You et al., 2012; Mao, 2016; Beheshtkhoo et al., 2018; Radini et al., 2018; Sangami and Manu, 2017). Typically, MTT assay is based on the mitochondrial activity, whose activity is usually stable in living cells. Correspondingly, change in activity of cells is linked to the mitochondrial activity. Work error is usually prevented

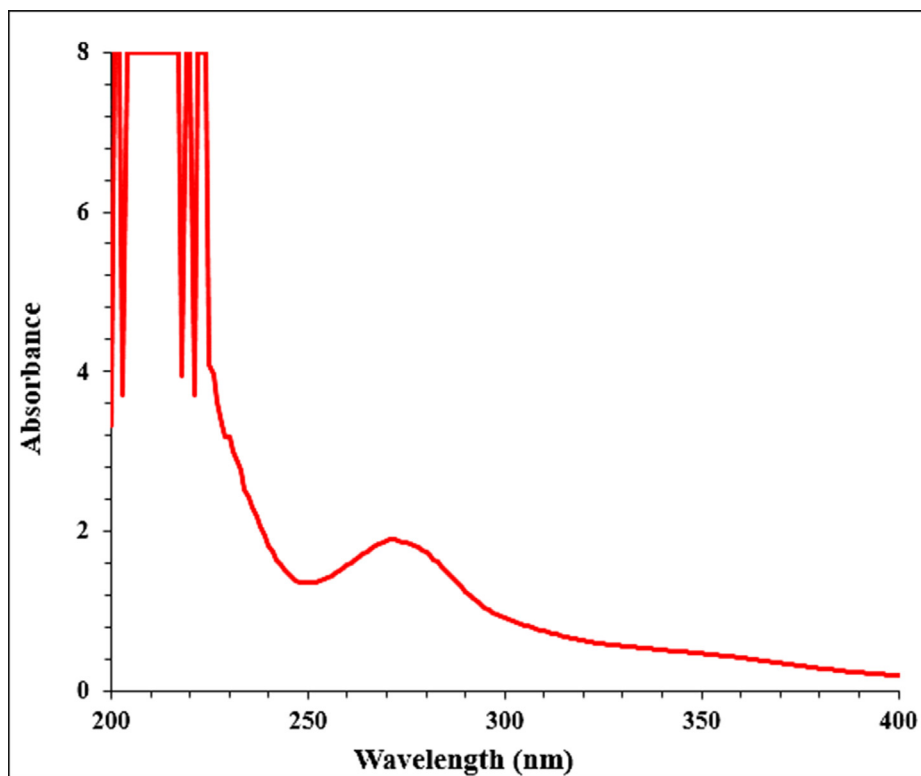


Fig. 1 UV-Vis analysis of FeNPs.

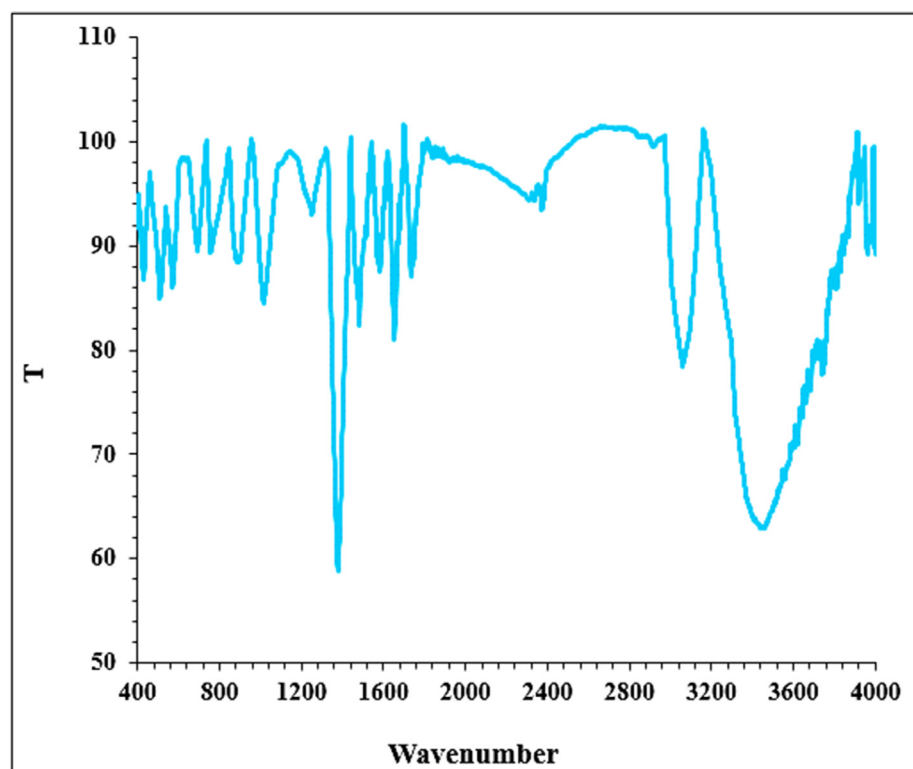


Fig. 2 FT-IR Spectrum of FeNPs synthesized using *Centaurea alba* extract.

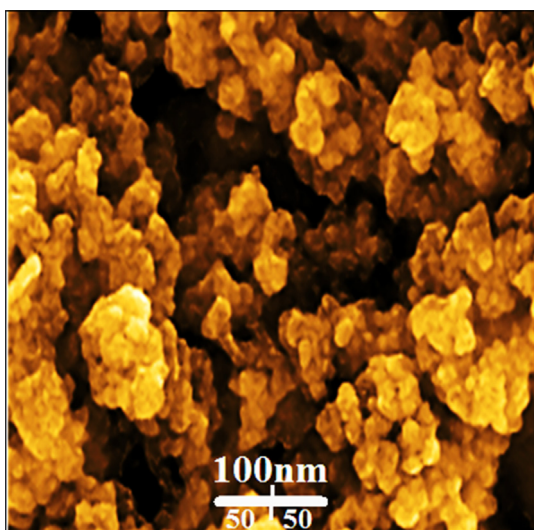


Fig. 3 FESEM image of FeNPs.

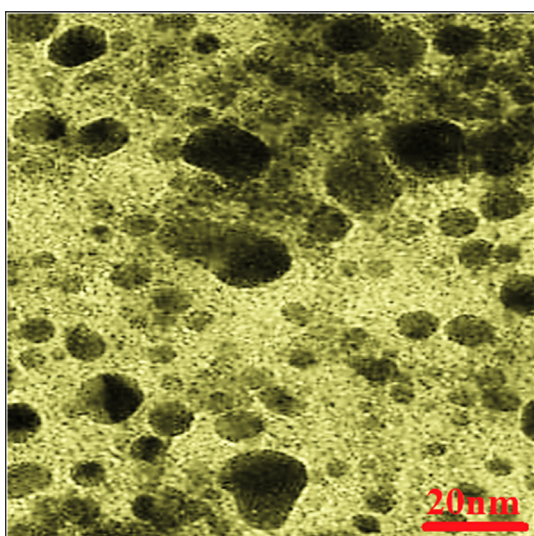


Fig. 4 TEM image of FeNPs.

in MTT assay, as the washing and shrinking steps are eliminated (Katata-Seru et al., 2018; Sankar et al., 2014; Namvar et al., 2014).

In this study, the cells (HUVEC) were treated with FeNPs in different concentrations and the resultant toxicity has been assessed by MTT assay for 48 h.

The absorbance rate was evaluated at 570 nm, which represented viability on normal cell line (HUVEC) even up to 1000 $\mu\text{g/mL}$ for FeNPs (Fig. 5).

Antioxidant property of the green synthesized FeNPs has been evaluated by DPPH test as a common free radical. Free radicals are highly reactive unstable molecules or atoms with a free electron, which is formed as a result of a bond breakage (Abdoli et al., 2020; Sujayev et al., 2020; Hummers and Offeman, 1958; Kooti et al., 2017; Shaneza, 2018). The main important FR in humans is O_2 . Oxygen molecules in the biological systems are generally exposed to various harsh environmental conditions such as stress, radiation, smoke etc, which

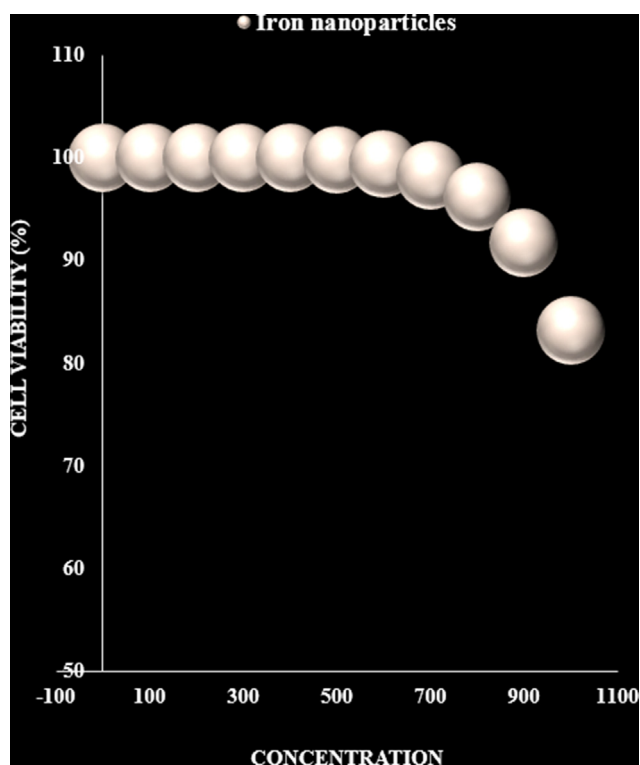


Fig. 5 The cytotoxicity effects of iron nanoparticles against normal (HUVEC) cell line.

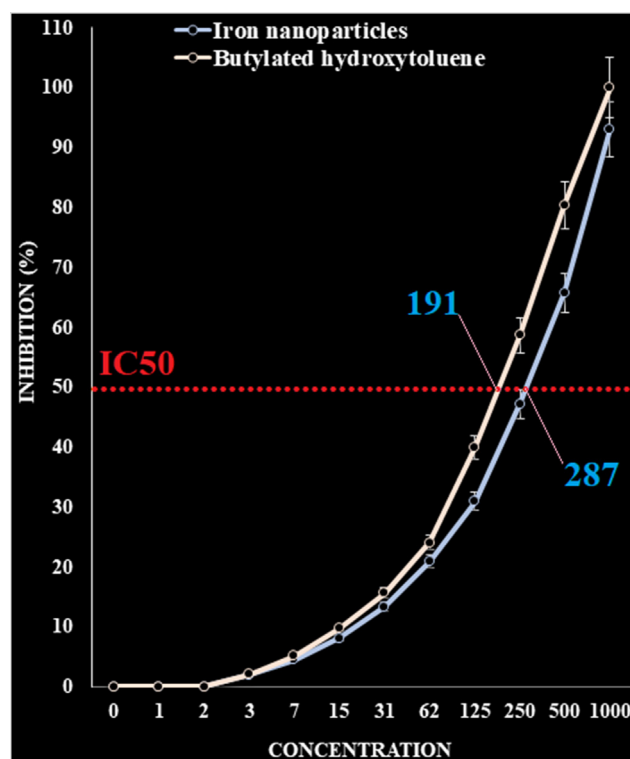


Fig. 6 The antioxidant activities of iron nanoparticles and BHT against DPPH.

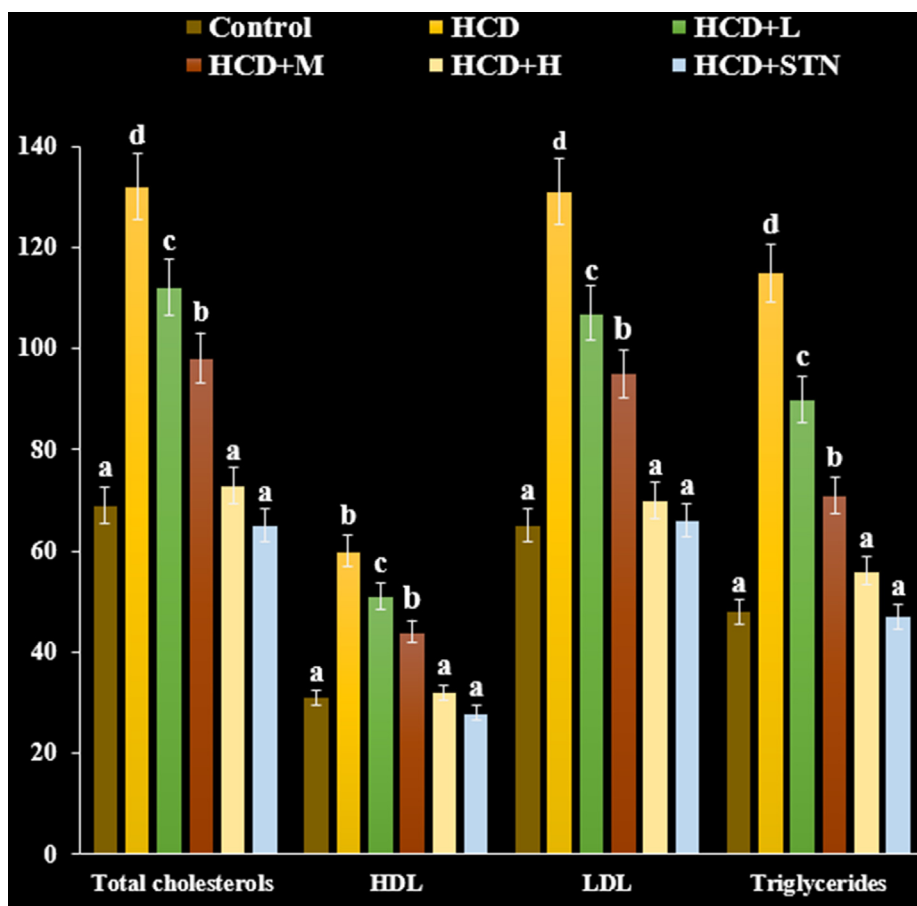


Fig. 7 Effects of FeNPs on plasma lipid profile concentration ((mg dL⁻¹) after six months in control and experimental animals (n = 6). HCD: High cholesterol diet, HCD + L: Low dose (100 µg kg⁻¹) of FeNPs, HCD + M: Medium dose (200 µg kg⁻¹) of FeNPs, HCD + H: High dose (400 µg kg⁻¹) of FeNPs, and HCD + STN: Atorvastatin (10 mg kg⁻¹) group.

leads to the production of free radicals and eventually destroys other molecules, compounds and DNA. Antioxidants are generally used to fight those free radicals from damaging (Abdoli et al., 2020). Antioxidants are substance that eliminate the threat of free radicals by inhibiting their production or transforming them into less reactive forms. In our immune system, as a part of inflammatory response, huge number of free radicals are produced by phagocytes, macrophages and neutrophils to fight against pathogens (Abdoli et al., 2020; Sujayev et al., 2020; Hummers and Offeman, 1958). Here, the presence of antioxidants are considered inevitable to prevent any harmful effects against the immune cells (Sujayev et al., 2020; Kooti et al., 2017). Natural antioxidants are found in legumes, fruits and vegetables, which are classified as dietary antioxidants and potentially reduce disease (Sujayev et al., 2020; Hummers and Offeman, 1958; Kooti et al., 2017; Shaneza, 2018). Even though synthetic antioxidants are such as BHT are being produced, they also possess comes up with carcinogenic and hepatotoxic effects. This lead to the reversal of attention to natural resources (Abdoli et al., 2020; Sujayev et al., 2020; Hummers and Offeman, 1958; Kooti et al., 2017; Shaneza, 2018; Arunachalam, 2003). Fig. 6 represents the scavenging capacity

of green synthesized FeNPs and BHT at different concentrations.

In the antioxidant test, the IC₅₀ of FeNPs and BHT against DPPH free radicals were 287 and 191 µg/mL, respectively (Fig. 6).

Feeding rats with high cholesterol supplemented diet resulted in a significant increase in plasma cholesterol, LDL and HDL levels (Fig. 7). The LDL and cholesterol level ($P \leq 0.01$) reduced after administration of FeNPs and STN in test groups. Moreover, treatment with STN (10 mg kg⁻¹) significantly reduced TC level (Fig. 7), ($P \leq 0.01$).

In HCD group, the blood triglyceride levels increased significantly compared to control rats ($P \leq 0.01$) (Fig. 7). However, the treatment group exhibited decrease in blood glucose level.

The media and intima thickness of the thoracic aortas from different groups were depicted in Fig. 8. It could be observed from the Fig. 8 that the intimal surface of aorta is smooth, whereas it is found to be intact in the control group. In HCD group, both the intimal and medial layers of aorta showed abnormalities. Furthermore, an increase in diameter in aortic wall was observed upon chronic HCD consumption.

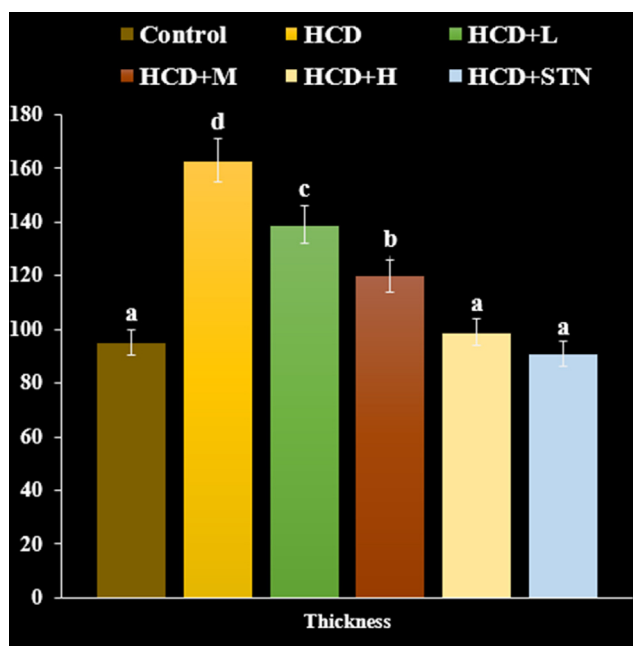


Fig. 8 Measurements of intima and media layers thickness (μm) of thoracic aortas from rats treated with or without FeNPs ($n = 6$). HCD: High cholesterol diet, HCD + L: Low dose ($100 \mu\text{g kg}^{-1}$) of FeNPs, HCD + M: Medium dose ($200 \mu\text{g kg}^{-1}$) of FeNPs, HCD + H: High dose ($400 \mu\text{g kg}^{-1}$) of FeNPs, and HCD + STN: Atorvastatin (10 mg kg^{-1}) group.

The treated group exhibited no significant changes in the histological appearance of aorta, which was very similar to STN and control group. However, the HCD group exhibited medial thickness and vascular fibrosis in the coronary artery wall, which was characterized by appearance of high density blue colour fiber. In $400 \mu\text{g kg}^{-1}$ treated group, vascular fibrosis and blue density were lowered (Fig. 8).

Lesions were observed in the medial and intimal layers of HCD group in the microscopic examination of aortic tissue. Atherosclerotic plaques initially develop as intimal precursor lesions at sites which are predisposed to lesion formation (Bentzon et al., 2014). Based on the microscopical pathology, atherosclerotic lesions were categorized into 6 class. Type I and II were classified as fatty streak precursor lesions. Type III has been classified as transition state lesions, which leads to type IV and Type V has the features of fibrosis and calcification, which is known as the complicated plaque. Type VI is found with fissure, surface thrombi with or without plaque rupture, surface erosions and plaque hematomas (Stary et al., 1995; Stary, 2000). Rats have been known as cholesterol resistant laboratory animals (Park et al., 2005). To overcome this tolerance, along with HCD, we inhibit the secretion of thyroid hormones by PTU. Since thyroid hormone directly promotes cholesterol metabolism by liver, PTU induces high blood levels of cholesterol (Wang et al., 2014).

4. Conclusion

The goal of this research work is to produce green FeNPs using *Centaurea alba* extract and to investigate the anti-atherosclerotic properties of iron nanoparticles. Many factors

are involved in the synthesis of green FeNPs. These factors include temperature, time of reaction, concentration of iron salt solution and volume ratio of extract solution to Iron solution. During the experiments, the optimal synthesis conditions were selected as: 60°C , 30 min, 0.001 M iron salt solution concentration and 1.5 mL volume ratio of extract solution to Iron solution. SEM and TEM analyses also showed that nanoparticles have a spherical morphology. Moreover, the average nanoparticle size is below 100 nm, which was indicated in SEM and TEM images.

The FeNPs showed the best antioxidant activities against DPPH. The IC_{50} of FeNPs and BHT against DPPH free radicals were 287 and $191 \mu\text{g/mL}$, respectively. According to the results of the *in vivo* condition, it can be concluded that FeNPs lowers LDL and prevents from early atherosclerotic changes in heart vessel wall and aorta. After clinical study, FeNPs containing plant leaf aqueous extract can be utilized as an efficient drug in the treatment of atherosclerosis in humans.

Funding (Name of fund, subsidy number): Science Foundation of the First People's Hospital of Zhaoqing This research was funded by the Researchers Supporting Project Number (RSP-2021/144), King Saud University, Riyadh, Saudi Arabia.

Declaration of Competing Interest

The authors declare that they have no known competing financial interests or personal relationships that could have appeared to influence the work reported in this paper.

Acknowledgement

The authors would like to extend their sincere appreciation to the Researchers Supporting Project Number (RSP-2021/144), King Saud University, Riyadh, Saudi Arabia.

References

- Nemorosa, S., 2017. '6 Th National Congress on Medicinal Plants Tehran, Iran 6 Th National Congress on Medicinal Plants Tehran. Iran' 13 (May), 104–111.
- Mosaddegh, M., Tavakoli, M., Behzad, S., 2018. Constituents of the aerial parts of *Centaurea behen*. *Chem. Nat. Compd.* 54 (5), 1015–1017.
- Fatima, Gulnar, et al. "Health Promoting Properties of Behman safed, a root of *Centaurea behen* Linn.-A Review." *Journal of Drug Delivery and Therapeutics* 9.4-s (2019): 657-660..
- Bensouici, C. et al, 2012. Sesquiterpene lactones and flavonoids from *Centaurea foucauldiana*. *Chemistry of Natural Compounds* 48 (3), 510–511.
- Öksüz, S., Ayyildiz, H., 1986. Sesquiterpene lactones from *Centaurea coronopifolia*. *Phytochemistry* 25 (2), 535–537.
- Oksuz, S. et al, 1982. A guaianolide from *Centaurea behen*. *Phytochemistry* 21 (11), 2747–2749.
- Esmaili, A. et al, 2013 (2013).. Antioxidant activity and isolation of luteoline from *Centaurea behen* L. grown in Iran. *J. Chem.* 2013.
- Harper, D., 2002. Talking about pictures: A case for photo elicitation. *Visual studies* 17 (1), 13–26.
- Khan, A.N. et al, 2011. Potent anti-platelet constituents from *Centaurea iberica*. *Molecules* 16 (3), 2053–2064.
- (a) Ghashghaii, A., Hashemnia, M., Nikousefat, Z., Zangeneh, M.M., Zangeneh, A., 2017. *Pharmaceutical Sciences* 23, 256-263. (b) Goorani, S., Shariatifar, N., Seydi, N., Zangeneh, A., Moradi, R., Tari, B., Nazari, F., Zangeneh, M.M., 2019. *Oriental Pharmacy and Experimental Medicine* 19, 403-413. (c) Jalalvand, A.R.,

- Zhaleh, M., Goorani, S., Zangeneh, M.M., Seydi, N., Zangeneh, A., Moradi, R., 2019. Journal of Photochemistry and Photobiology B: Biology 192, 103-112.
- (a) Abdoli, M., Sadrjavadi, K., Arkan, E., Zangeneh, M.M., Moradi, S., Zangeneh, A., Shahlaei, M., Khaledian S. 2020. J Drug Deliv Sci Technol. 60, 102044. (b) Dou, L., Zhang, X., Zangeneh, M.M., Zhang, Y. 2020. Bioorg. Chem. 106: 104468. (d) Han, Y., Gao, Y., Cao, X., Zangeneh, M.M., Liu, S., Li, J. 2020. Int. J. Biol. Macromol. 164: 2974-2986. (e) Ishaq, M., Taslimi, P., Shafiq, Z., Khan, S., Salmas, R.E., Zangeneh, M.M., Saeed, A., Zangeneh, A., Sadeghian, N., Asari, A., Mohamad, H. 2020. Bioorg. Chem. 100: 103924. (f) Li, Y., Li, N., Jiang, W., Ma, G., Zangeneh, M.M., 2020. Int. J. Biol. Macromol. 163: 2162-2171.
- (a) Sujayev, A., Taslimi, P., Garibov, E., Karaman, M., Zangeneh, M. M., 2020. Bioorg. Chem. 104: 104216. (b) Sun, T., Gao, J., Shi, H., Han, D., Zangeneh, M.M., Liu, N., Liu, H., Guo, Y., Liu, X., 2020. Int. J. Biol. Macromol. 165: 787-795. (c) Tahvilian, R., Zangeneh, M.M., Falahi, H., Sadrjavadi, K., Jalalvand, A.R., Zangeneh, A., 2019. Applied Organometallic Chemistry 33, e5234.
- Hummers, W.S., Offeman, R.E., 1958. J. Am. Chem. Soc. 80, 1339.
- Kooti, W., Servatyari, K., Behzadifar, M., et al, 2017. Effective Medicinal Plant in Cancer Treatment, Part 2: Review Study. J Evid Based Complementary Altern Med. 22 (4), 982-995. <https://doi.org/10.1177/2156587217696927>.
- Shaneza, A. et al, 2018. Herbal treatment for the ovarian cancer. SGVU J. Pharmaceutical Research & Education 3 (2), 325-329.
- Arunachalam, K.D. et al, 2003. One-step green synthesis and characterization of leaf extract-mediated biocompatible silver and gold nanoparticles from Memecylon umbellatum. Int. J. Nanomedicine. 8, 1307-1315.
- Pashaie, B., Hobbenaghi, R., Malekinejad, H., 2017. Anti-atherosclerotic effect of *Cynodon dactylon* extract on experimentally induced hypercholesterolemia in rats. Vet Res Forum. 8 (3), 185-193.
- El-Moslamy, S.H. et al, 2017. Applying Taguchi design and large-scale strategy for mycosynthesis of nano-silver from endophytic *Trichoderma harzianum* SYA. F4 and its application against phytopathogens. Sci. Rep. 7 (1), 1-22.
- Karpagavinayagam, P., Vedhi, C., 2019. Green synthesis of iron oxide nanoparticles using *Avicennia marina* flower extract. Vacuum 160, 286-292.
- Yazdani, M. et al, 2019. Improvement of biogas production from slaughterhouse wastewater using biosynthesized iron nanoparticles from water treatment sludge. Renewable Energy 135, 496-501.
- Ting, A.S., Yien, and Jia En Chin, 2020. Biogenic synthesis of iron nanoparticles from apple peel extracts for decolorization of malachite green dye. Water Air Soil Pollut. 231, 1-10.
- Fazlzadeh, Mehdi et al, 2017. A novel green synthesis of zero valent iron nanoparticles (NZVI) using three plant extracts and their efficient application for removal of Cr (VI) from aqueous solutions. Adv. Powder Technol. 28 (1), 122-130.
- Katata-Seru, Lebogang et al, 2018. Green synthesis of iron nanoparticles using *Moringa oleifera* extracts and their applications: removal of nitrate from water and antibacterial activity against *Escherichia coli*. J. Mol. Liq. 256, 296-304.
- Alam, Tariq et al, 2019. Biogenic synthesis of iron oxide nanoparticles via *Skimmia laureola* and their antibacterial efficacy against bacterial wilt pathogen *Ralstonia solanacearum*. Mater. Sci. Eng., C 98, 101-108.
- Devatha, C.P., Jagadeesh, K., Patil, Mallikarjun, 2018. Effect of Green synthesized iron nanoparticles by *Azadirachta Indica* in different proportions on antibacterial activity. Environ. Nanotechnol. Monit. Manage. 9, 85-94.
- Önal, Emel Simla et al, 2017. Green synthesis of iron nanoparticles by aqueous extract of *Eriobotrya japonica* leaves as a heterogeneous fenton-like catalyst: degradation of basic red 46. Int. J. Chem. Eng. Appl. 8, 327-333.
- Bibi, Ismat et al, 2019. Green synthesis of iron oxide nanoparticles using pomegranate seeds extract and photocatalytic activity evaluation for the degradation of textile dye. J. Mater. Res. Technol. 8 (6), 6115-6124.
- (a) Veisi, H.; Tamoradi, T.; Karmakar, B. Mohammadi, P.; Hemmati, S.; Mat. Sci. Eng. C. 104 (2019) 109919; (b) M. Hamelian, K. Varmira, H. Veisi, Journal of Photochemistry and Photobiology B: Biology 184 (2018) 71-79.
- Tahvilian, R., Zangeneh, M.M., Falahi, H., et al, 2019. Green synthesis and chemical characterization of copper nanoparticles using *Allium saralicum* leaves and assessment of their cytotoxicity, antioxidant, antimicrobial, and cutaneous wound healing properties. Appl Organometal Chem. 33, <https://doi.org/10.1002/aoc.5234> e5234.
- You, C., Han, C., Wang, X., et al, 2012. The progress of silver nanoparticles in the antibacterial mechanism, clinical application and cytotoxicity. Mol. Biol. Rep. 39, 9193-9201. <https://doi.org/10.1007/s11033-012-1792-8>.
- Mao, B.H. et al, 2016. Mechanisms of silver nanoparticle-induced toxicity and important role of autophagy. Nanotoxicol. 10, 1021-1040.
- Beheshtkhou, N., Kouhbanani, M.A.J., Savardashtaki, A., et al, 2018. Green synthesis of iron oxide nanoparticles by aqueous leaf extract of *Daphne mezereum* as a novel dye removing material. Appl. Phys. A 124, 363-369.
- Radini, I.A., Hasan, N., Malik, M.A., et al, 2018. Biosynthesis of iron nanoparticles using *Trigonella foenum-graecum* seed extract for photocatalytic methyl orange dye degradation and antibacterial applications. J. Photochem. Photobiol., B 183, 154-163.
- Sangami, S., Manu, M., 2017. Synthesis of Green Iron Nanoparticles using Laterite and their application as a Fenton-like catalyst for the degradation of herbicide Ametryn in water. Environ. Technol. Innov. 8, 150-163.
- Katata-Seru, L., Moremedi, T., Aremu, O.S., et al, 2018. Green synthesis of iron nanoparticles using *Moringa oleifera* extracts and their applications: Removal of nitrate from water and antibacterial activity against *Escherichia coli*. J. Mol. Liq. 256, 296-304.
- Sankar, R., Maheswari, R., Karthik, S., et al, 2014. Anticancer activity of *Ficus religiosa* engineered copper oxide nanoparticles. Mat Sci Eng C 44, 234-239.
- Namvar, F., Rahman, H.S., Mohamad, R., et al, 2014. Cytotoxic effect of magnetic iron oxide nanoparticles synthesized via seaweed aqueous extract. Int. J. Nanomedicine 19, 2479-2488.
- Bentzon, J.F., Otsuka, F., Virmani, R., et al, 2014. Mechanisms of plaque formation and rupture. Circ. Res. 114 (12), 1852-1866.
- Sary, H.C., Chandler, A.B., Dinsmore, R.E., et al, 1995. A definition of advanced types of atherosclerotic lesions and a histological classification of atherosclerosis. Circulation 92 (5), 1355-1374.
- Sary, H.C., 2000. Natural history and histological classification of atherosclerotic lesions: An update. Arterioscler. Thromb. Vasc. Biol. 20 (5), 1177-1178.
- Park, K., Son, H., Kim, S.W., et al, 2005. Initial validation of a novel rat model of vasculogenic erectile dysfunction with generalized atherosclerosis. Int. J. Impot. Res. 17 (5), 424-430.
- Wang, P., Xu, T.-Y., Guan, Y.-F., et al, 2014. Vascular smooth muscle cell apoptosis is an early trigger for hypothyroid atherosclerosis. Cardiovas Res. 102 (3), 448-459.